Laser and Particle Beams (1998), *vol.* 16, *no.* 2, *pp.* 397–404
Printed in the United States of America

Study of second harmonic emissions for characterization of laser–plasma X-ray sources

By A. GIULIETTI, C. BENEDUCE, T. CECCOTTI,[1] D. GIULIETTI,[2] L.A. GIZZI, AND R. MILDREN
Istituto di Fisica Atomica e Molecolare, Via del Giardino, 7, Pisa, 56127, Italy

(Received 23 October 1996; Accepted 23 January 1998)

An investigation of second harmonic (SH) and X-ray emissions from Al plasmas produced by 3-ns, 1.064-μm laser pulses at 10^{14} W/cm^2 is reported. The SH and X-ray yields are strongly correlated as a function of the target position with respect to the laser beam focus. The SH originates from the underdense coronal plasma and has a filamentary source, while the X-ray source is uniform. The results suggest that, although the X-ray emission is significantly enhanced by the filamentation of the laser light in the corona, there is a *smoothing* effect in the energy transport process toward the overdense region.

1. Introduction

At temperatures of hundreds of eVs, which is typical of laser-produced plasmas (LPP), the energy emitted in the X-ray region of the spectrum is a relevant percentage of the absorbed laser energy. While the laser energy is absorbed in the underdense plasma ($n_e < n_c$, where $n_c = m\omega^2/4\pi e^2$ is the critical density for the electromagnetic radiation of the angular frequency ω), most of the X-ray emission is generated in the overdense region. Thus, the study of energy transport from the underdense to the dense regions of the plasma is relevant to both basic plasma physics and the optimization of laser-produced X-ray sources. It is well known that the X-ray conversion efficiency increases when shorter laser wavelengths are used, to keep the absorption region close to the X-ray emitting layer. However, investigations with near-infrared lasers are relevant for two distinct reasons: (1) many practical X-ray sources operate in this regime; and (2) in this condition the laser–plasma interaction region is well decoupled from the main X-ray generating layers, allowing more accurate measurements on the effects related to each region as well as on their interplay. In addition, due to the lower threshold intensities for nonlinear processes, longer wavelength laser light gives rise to more efficient production of hot electrons and therefore to brighter X-ray emissions in the harder ($\approx$10-keV) region.

A recent experiment (Macchi *et al.* 1996) with 1-μm laser light suggested that the X-ray conversion efficiency is enhanced by the filamentation instability (FI). A useful diagnostic for studying the FI is supplied by second harmonic (SH) emissions. In fact, SH emission sources are localized into density and intensity inhomogeneities (Schifano *et al.* 1994; Stamper *et al.* 1986). Previous measurements (Biancalana *et al.* 1993) based on SH emissions have indeed shown that the FI causes the laser beam to break into several beamlets due to a positive feedback between laser hot spots and channels in the electron density (Sodha *et al.* 1976).

All of these experiments demonstrate that simultaneous measurements of SH and X-ray emission provide invaluable information on the physics of laser interaction with plasmas. This

[1]Present address: Universitè Paris VI, France
[2]Also at Dipartimento di Fisica, Università di Pisa, Italy

 0263-0346/98 $12.50

method also was recently used for the study of X-ray emissions from ultrashort pulse laser irradiations of solid targets (Gizzi *et al.* 1996), also showing in that case very interesting correlations in spite of the different interaction regimes.

In this paper we report on an investigation of both second harmonic and X-ray emissions from a plasma produced by a 3-ns, 10^{14}-W/cm^2 laser pulse focused on a massive aluminum target. SH and X-ray emissions were studied as a function of the target position with respect to the laser beam focus. Imaging techniques were used to analyze the structures of the SH and X-ray sources. Finally, time-resolved analysis of the SH emission and $3\omega/2$ also was carried out. The experimental setup is described in section 2, while results are presented and discussed in section 3.

2. Experimental setup

The experimental setup is shown in figure 1. An Nd-laser ($\lambda = 1.064\ \mu$m) delivering 1.5 J on a target in 3-ns pulses was used. The laser energy, pulse shape, and focal spot were monitored shot-by-shot by using a fast photodiode, a calorimeter, and an equivalent plane CCD, respectively. The laser operated in a single-transverse, multiple-longitudinal mode. Consequently,

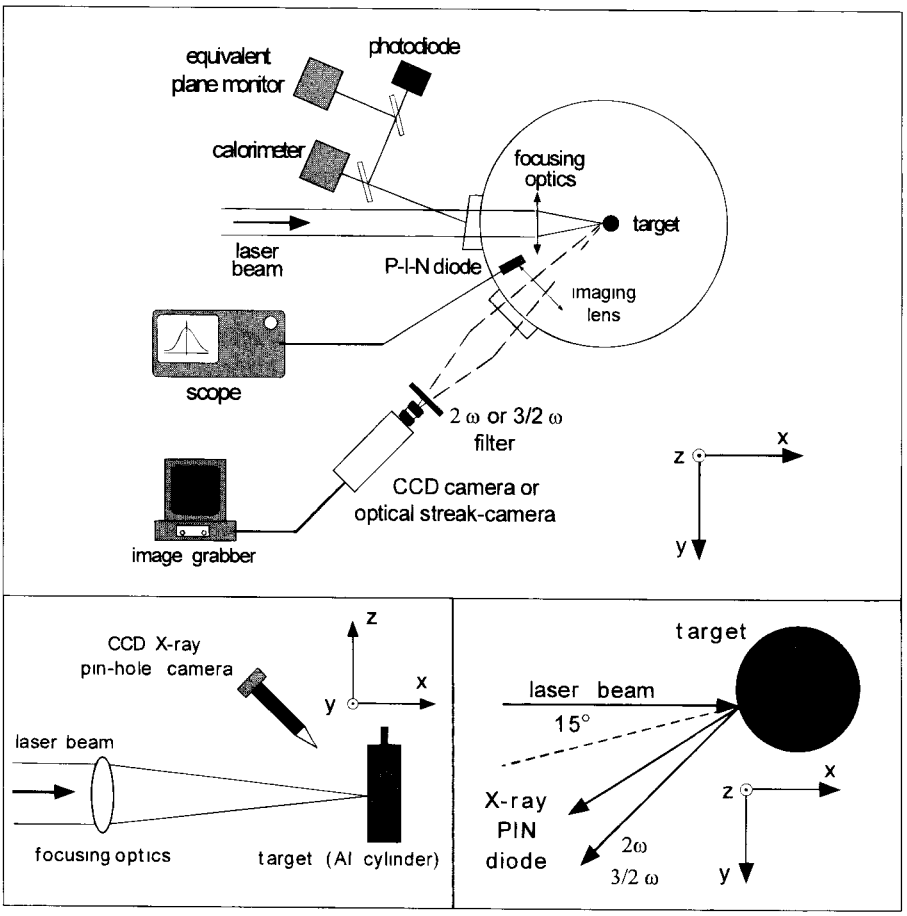

FIGURE 1. Layout of the experimental setup (top). In the boxes at the bottom are shown the pinhole camera setting, and the geometry of the experiment.

the laser emission was strongly modulated in time by nonreproducible spikes whose mean duration was measured to be about 50 ps, as expected from mode beating in the oscillator cavity.

The laser beam was focused on target by an $f/8$ optics at an incidence angle of 15° to avoid backreflections. The FWHM spot size without plasma was measured by an equivalent plane monitor and was found to be approximately 24 μm. Therefore, the nominal irradiance on the target was about 10^{14} W/cm^2.

The X-ray emission was detected at 30° from the laser beam axis, by using an X-ray PIN diode, filtered by an 8-μm Beryllium foil. Taking into account the transmittivity of the Beryllium filter and the spectral sensitivity of the PIN diode, the investigated X-ray spectral region was in the 1–10-KeV range. The maximum of the overall sensitivity was at ≈1.7 keV. Time-integrated images of the X-ray source were taken by using a CCD pinhole camera (as shown in figure 1b) filtered with an 8-μm Beryllium foil. The spatial resolution, which is determined by the pinhole size, was 13 μm.

The SH radiation emitted at 45° was collected by an $f/5$ optics and analyzed in different ways. First, time-integrated images of the plasma were formed on a CCD after passing the light emitted by the plasma through a narrow band (≈30 Å) interference filter centered at ≈5320 Å. The resolution of the imaging optics was estimated to be of the order of 10 μm. Second, a fraction of the SH light was sent to a photomultiplier to measure the amplitude of the SH signal. Third, time-resolved SH images of the plasma were formed directly on the slit of an optical streak camera to perform 1D time-resolved imaging. Alternatively, an optical spectrometer was coupled to the streak camera to perform time-resolved spectroscopy of the SH emission with a spectral resolution of ≈2 Å. The same measurements were also performed on $3\omega/2$ emission by using an interference filter centered at ≈7090 Å.

3. Experimental results

3.1. *X-ray and SH yield measurements*

The two plots in figure 2 show the X-ray and SH intensities as a function of the target position with respect of the laser beam focal plane ($x = 0$), with x increasing in the direction of propagation of the laser beam. The position of the focal plane was determined with an uncertainty of ±200 μm. Both the SH and X-ray emission intensities vary considerably when the target is moved within a ±2-mm range from the focal plane; both intensities show a minimum for the zero target position and show maxima between −1 and −0.5 mm on one side and 0.5 on the opposite side. A similar behavior was observed in previous measurements on SH emissions (Biancalana *et al.* 1993); in that work, a strong correlation between the SH generation and the onset of filamentation was proved experimentally. The present measurements provide evidence of a strong correlation between the SH and soft X-ray emissions.

3.2. *Identification of SH sources*

The sources of SH emission were identified by using two different techniques based on imaging and spectroscopic measurements, respectively.

First, the plasma was imaged at 45° with respect to the beam axis (i.e., 30° from the plasma expansion axis) in both 2ω and $3\omega/2$ lights on the slit of the optical streak camera. The slit was set to select a given slice of the image to investigate the corresponding plasma region. Figure 3 shows the streak images of three different regions in 2ω and $3\omega/2$ lights. Both 2ω and $3\omega/2$ show a spiky structure in time with a poor shot-by-shot reproducibility.

Figure 3 clearly shows that the overall intensity of $3\omega/2$ emission decreases strongly as plasma regions farther from the target are selected. We recall that $3\omega/2$ harmonic emission is

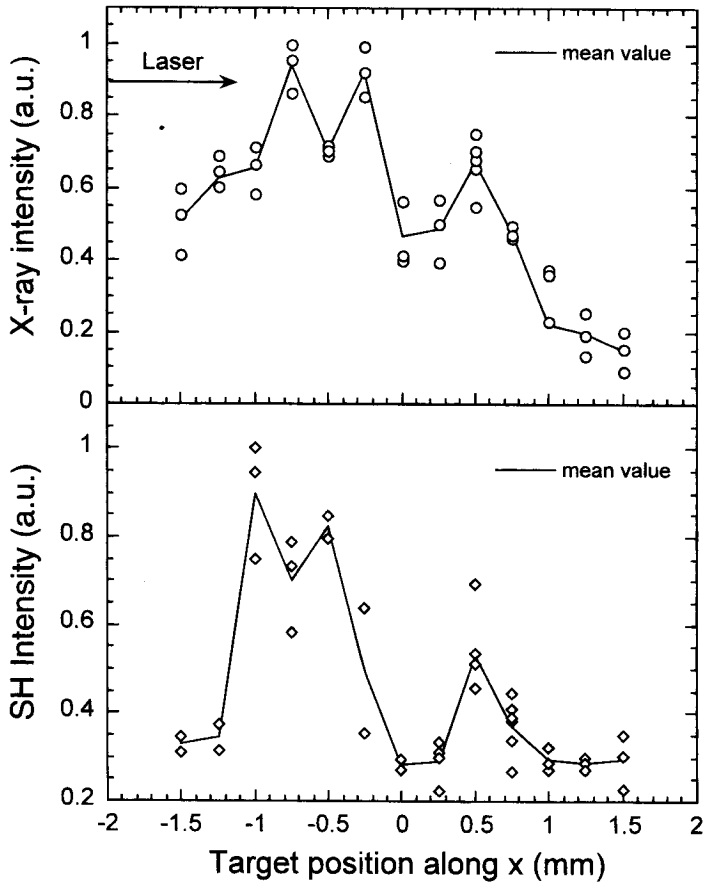

FIGURE 2. X-ray (top) and SH (bottom) intensities as a function of the target position with respect to the laser beam focal plane.

a signature of the $n_c/4$ electron density layer in the plasma (see Giulietti *et al.* 1993 and references therein). Such a dramatic reduction in the intensity is not observed in the case of SH emission. Moreover, SH radiation is emitted from a broader plasma region than the $3\omega/2$ radiation. Once the line of view of the detector is taken into account, these observations show that the region from which SH originates is wider than the $3\omega/2$ emitting layer ($\approx n_c/4$) and that the SH emitting region is characterized by an electron density that is less than $n_c/4$.

Another measurement involved time-resolved spectroscopy of the SH emission. All of the time-resolved spectra showed that the emitted SH radiation was shifted from the exact $2\omega_0$ frequency and broadened in comparison with the width of the purely doubled frequency radiation. A typical time-resolved spectrum is shown in figure 4.

Such spectra were interpreted in terms of the theory introduced by Stamper *et al.* (1985) and proved experimentally by Giulietti *et al.* (1989). According to this theory, the generation of substantial SH emissions in filamentary plasmas requires the existence of either a reflected or a stimulated Brillouin backscattered (SBS) wave within the filament. For backward-emitted SH (which is close to our experimental condition) the frequency of the SH radiation is $\omega_b + \omega_b$, where ω_b is the frequency of the Brillouin backscattered wave and the shift can be written as:

$$\left(\frac{\Delta\omega}{\omega}\right)_{2\omega_0} = \left(\frac{\Delta\omega}{\omega}\right)_{\omega_0} \approx \frac{2}{c}(v_s + v_p), \tag{1}$$

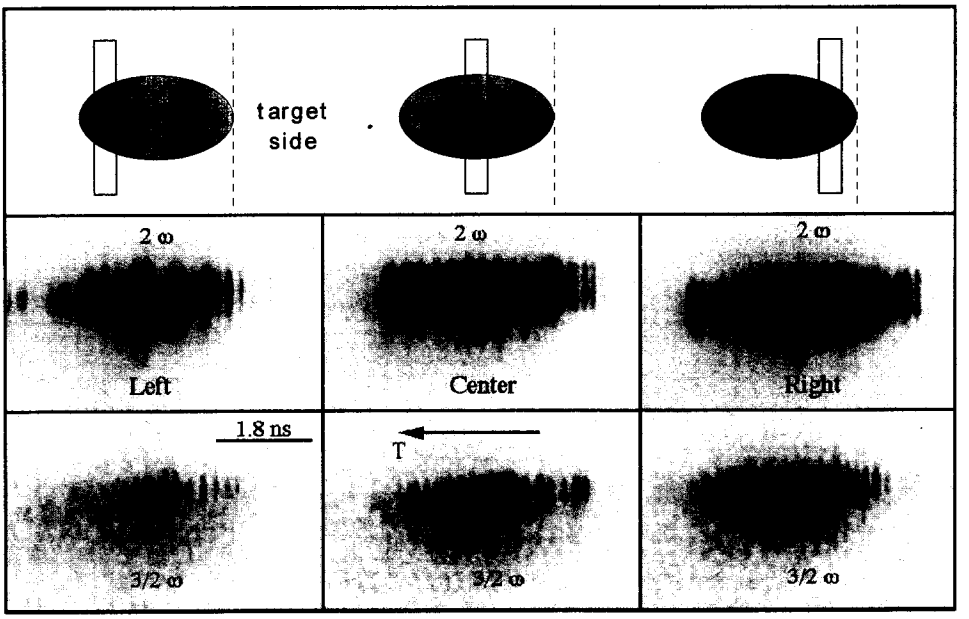

FIGURE 3. Time-resolved (streaked in the direction of the arrow) images in 2ω and $3\omega/2$ light of three different regions of the plasma.

where $v_s = 1.5 \cdot 10^7$ cm/s is the speed of the ion-acoustic wave (assuming that $T_e = 500$ eV) and v_p is the flow velocity of the plasma. Using equation (1), from the observed spectral shift we obtain $9.4 \cdot 10^6$ cm/s $< v_p < 1.9 \cdot 10^7$ cm/s. By comparing the values of the flow velocity obtained from the SH spectra with the hydrodynamic simulations of the 1D hydrocode MEDUSA (Christiansen *et al.* 1974; Rodgers *et al.* 1989), the region of dominant SH emission can be located at 80 μm from the critical layer, where the electron density ranges between 1.4 and $2.0 \cdot 10^{20}$ cm^{-3}. These values must be considered only as an estimate of the order of magnitude, because of the limits of applicability of the simulation code set by the 1D approximation for the plasma motion. In fact, the 1D approximation leads to an underestimation of the adiabatic cooling of the plasma during expansion, as well as an overestimation of the density scale length and the consequent laser energy absorption. However, since the simulation is likely to over-

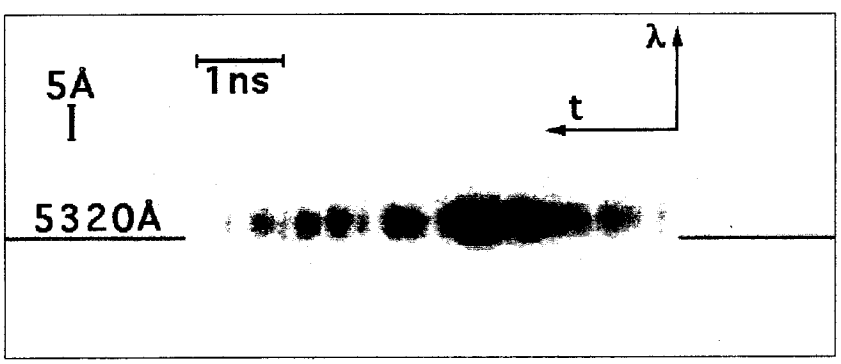

FIGURE 4. Time-resolved SH spectrum. The horizontal lines indicate the calibrated position for the 5320-Å wavelength.

estimate both the density and the velocity in a given point in space, these values give an upper limit to the density of the SH emitting region. Thus we conclude that SH emission definitely comes from a region with a density below $n_c/4$, in agreement with the result previously obtained from the comparison of the 2ω and $3\omega/2$ images.

How the intense Brillouin backscattering required by our model may be activated is an interesting question. Considering that SH emission is observed in the region with $n_c/n_e < n_c/4$, an attractive hypothesis is that the SBS would be enhanced there by stimulated Raman scattering (SRS) via a decay process of the SRS-driven plasma wave. In this case, SH could be the signature of SRS, via SRS-enhanced SBS in filaments, rather than nonenhanced SBS in filaments. In this scenario, filaments also may extend beyond the $n_c/4$ layer. Concerning the spiky behavior, which is already present in the laser pulse, it may be enhanced by the typical temporal modulation of the filaments themselves in the nonlinear regime of filamentation and/or by the interplay between the filamentation and SBS.

3.3. *Intensity distribution*

In this section we compare X-ray plasma images obtained by the pin hole camera with images of the plasma in SH light. X-ray images taken for different target positions ($-500 < x < +500$ μm) along the laser beam propagation axis show that the shape of the X-ray emitting region does not vary significantly. In contrast, the shape of the SH emitting region is found to change even for a small target displacement. The latter observation is consistent with previous measurements (Biancalana *et al.* 1993). These images are compared with the intensity distribution of the laser spot without plasma, shown in figure 5a, as obtained by equivalent plane imaging. The measured FWHM spot size was 24 μm, and the intensity distribution in the spot was found to be rather uniform within the resolution of ≈ 4 μm.

An SH image taken with the target in the position $x = 0$ is shown in figure 5b. The SH emission from the corona shows structures with a typical size of 10–20 μm. It is interesting to compare this scale length with the scale length of maximum growth for the filamentation instability in our plasma conditions. A detailed analysis would require a sophisticated simulation of nonstationary (possibly nonlinear) filamentation, which is beyond the aim of this work.

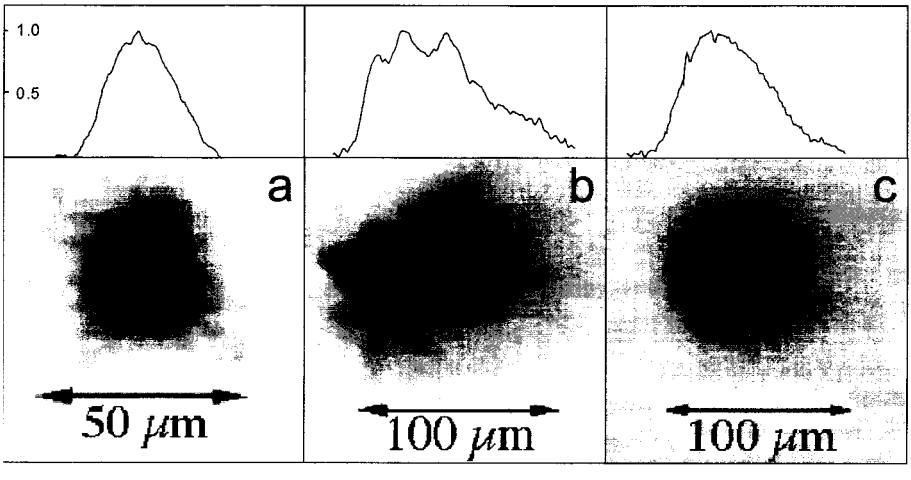

FIGURE 5. Images showing the intensity distribution and the corresponding lineouts for (a) the 1.06-μm-wavelength laser focal spot, (b) the SH source, and (c) the X-ray source.

Here we only give an estimate based on a detailed kinetic theory of thermal filamentation (Epperlein 1990).

According to this theory, the maximum growth rate $K_{\max}$ and the optimum perturbation wavelength $\lambda_{\max}$ are given by:

$$K_{\max} = 2\cdot 10^{-2}\ \mu\mathrm{m}^{-1}\ \frac{ZI_L^{3/4}(n_e/n_c)^{5/4}(\ln\Lambda)^{1/2}}{\epsilon^{7/8}T^{7/4}\phi^{7/4}(1+1/Z)^{1/2}}$$

$$\lambda_{\max} = 15\ \mu m\ \frac{\epsilon^{3/16}\lambda_L^{1/2}T^{7/8}\phi^{3/8}(1+1/Z)^{1/4}}{I_L^{3/8}(n_e/n_c)^{5/8}(\ln\Lambda)^{1/4}}, \tag{2}$$

where $\phi = (Z+0.24)/(1+0.24Z)$, I_L is the laser intensity in units of 10^{14} Wcm^2, λ_L is the laser wavelength in μm, T is the electron temperature in keV, ln Λ is the Coulomb logarithm, and ϵ is the plasma dielectric constant. Assuming that $T \approx 0.5$ keV, $I_L \approx 10^{14}$ Wcm^{-2}, $(n_e/n_c) \approx 10^{-1}$, we find, from relations (2), that $K_{\max} \approx 5\cdot 10^{-3}\ \mu\mathrm{m}^{-1}$ and $\lambda_{\max} \approx 10\ \mu$m. The estimated growth rate is consistent with the focal depth of our focusing optics, and the optimum perturbation wavelength agrees with the observed perturbation scale length.

Finally, figure 5c shows an X-ray pin hole camera image of the plasma with a resolution of 13 μm. In the limit of such a resolution, the X-ray emitting region is uniform, in spite of the filamentary distribution of SH emission in the corona.

A qualitative explanation for this result can be given by comparing the typical size of the inhomogeneities in SH emission with the mean free path of thermal electrons λ_e. According to the classical theory of thermal diffusion (Spitzer & Harm 1953), we have

$$\lambda_e \cong 1.5\cdot 10^{13}\ \mathrm{cm}\ \frac{T^2}{Zn_e \ln\Lambda}, \tag{3}$$

where T is in eV. Therefore, λ_e is found to range between 10 and 10^2 μm in the corona ($n_e \approx 10^{20}$ to 10^{21} cm^{-3}). Hence, any spatial inhomogeneity with a typical scale of 10 μm or less in the distribution of laser energy deposition in the corona will be "smoothed" out during the thermal energy transport toward the overdense region. However, it should be noted that the classical theory of thermal transport (which holds for plasmas produced by long, moderate intensity laser pulses, as in the present case) may become invalid if local, sharp density gradients are generated by the onset of FI. Thus the detailed mechanisms of thermal energy transfer from the corona to the denser plasma region should require a more detailed theoretical description.

4. Conclusion

SH emission was used as the main diagnostic of the laser–plasma interaction in a laser generated plasma X-ray source. SH intensity measurements and source imaging were proved to be effective tools for investigating a regime (1.06 μm, 3 ns, 10^{14} Wcm^{-2}, Al target) dominated by filamentation. Simultaneous measurements of SH and X-ray emissions for different positions of the target showed a strong correlation between the two emissions, with evidence that a higher level of filamentation corresponds to an increased laser-to-X-ray conversion efficiency. The region in which SH generation (and hence filamentation) takes place was identified to be the underdense corona, far from the overdense X-ray emitting region. The SH source was found to be divided into filaments, whose structures are very sensitive to the target position. On the contrary, the soft X-ray source was found to be rather smooth, and its uniformity was surprisingly almost unaffected by target displacements as large as several Rayleigh lengths of the focusing optics. This is consistent with previous observations showing that the dependence of the X-ray yield on target position is not due to a purely geometrical effect.

Moreover, we obtained evidence of a smoothing effect operated by the energy transport process from the coronal filamentary region to the dense plasma. Our study shows that a filamentary regime of laser–plasma interaction may be suitable for the production of a rather efficient, smooth source of soft X rays.

REFERENCES

BIANCALANA, V. *et al.* 1993 *Europhys. Lett.* **22**, 175.
CHRISTIANSEN, S.P. *et al.* 1974 *Comp. Phys. Comm.* **7**, 271.
EPPERLEIN, E.M. 1990 *Phys. Rev. Lett.* **65**, 2145.
GIULIETTI, A. *et al.* 1989 *Phys. Rev. Lett.* **63**, 524.
GIULIETTI, D. *et al.* 1991 *Il Nuovo Cimento D* **13**, 845.
GIZZI, L.A. *et al.* 1996 *Phys. Rev. Lett.* **76**, 2278.
MACCHI, A. *et al.* 1996 *Il Nuovo Cimento D* **18**, 727.
RODGERS, P.A. *et al.* 1989 RAL Report No. RAL-89-127, unpublished.
SCHIFANO, E. *et al.* 1994 *Laser Part. Beams* **12**, 435.
SODHA, M.S. *et al.* 1979 *Progr. Optics* **13**, 171.
SPITZER, L. & HARM, R. 1953 *Phys. Rev.* **89**, 977.
STAMPER, J.A. *et al.* 1985 *Phys. Fluids* **28**, 2563.